Effects of Dopants on the properties of $BiFeO_3$

Session 2013

SUBMITTED BY
SAMEEL NASIR
2013-MS-MME-02

SUPERVISOR
DR. MUHAMMAD ASIF RAFIQ

Department of Metallurgical and Materials Engineering
University of Engineering and Technology, Lahore

Effect of Dopants on the Properties of $BiFeO_3$

Thesis submitted to the University of Engineering & Technology, Lahore

For partial fulfilment of the requirements for the
Master's degree
In

Metallurgical and Materials Engineering

Approved on: _____

_____	_____
Dr. Muhammad Asif Rafiq (Internal Examiner)	External Examiner
_____	_____
Chairman, MME Deptt.	Dean, Faculty of CMPE

Department of Metallurgical & Materials Engineering
University of Engineering & Technology, Lahore

To Allah Almighty,
Who has been my eternal rock and source of refuge, and for His words in 61: 13" Nasrun min Allahi, wa fat'hun qareeb" that kept me all through the journey of completing this work. I also dedicate this work to my Family for being great pillars of support.

Declaration

It is hereby declared that this research, entitled "Effect of dopants on the properties of $BiFeO_3$" is an original and authentic work of the author. It is further guaranteed that current work is not submitted for the acquisition of any degree or qualification at any other institute besides University of Engineering & Technology, Lahore for the partial fulfilment of M.Sc. in Metallurgical and Materials Engineering degree requirement. It is assured that, this thesis does not contain any formerly published data except where the references are quoted.

SAMEEL NASIR

2013-MS-MME-02

Acknowledgments

In the name of ALLAH, the most beneficent and merciful who gave me the strength and knowledge to carry out this research and complete the project **"Effect of dopants on the properties of $BiFeO_3$"** My research work would not have been completed without the provision and assistance of many people. I would like to appreciate the Department of Metallurgical and Materials Engineering, University of Engineering and Technology Lahore for giving me the opportunity to instigate this research in the first place and for the financial and infrastructural support.

My deep gratitude and appreciation goes to my research supervisor **Dr. Muhammad Asif Rafiq** for his constant guidance, motivation and support during the course of my studies. His valuable suggestions broadened horizon and made this research work interesting and challenging for. I also like to acknowledge the contributions made by my fellows from whom I have learned so much.

I would also like to acknowledge the Departments of Physics, School of Science and engineering, Lahore University of Management science (LUMS) Lahore for extending the infrastructural and laboratory facilities.

Table of Contents

List of Abbreviations

AFM	Antiferromagnets
BFO	Bismuth Ferrite
CIS	Complex Impedance Spectroscopy
eV	Electron volt
FE	Ferroelectric
FM	Ferromagnetic
FTIR	Fourier Transform Infrared Spectroscopy
LCR Meter	Inductance, Capacitance & Resistance meter
M	Modulus
M′	Real Part of Modulus
M″	Imaginary Part of Modulus
ME	Magnetoelectric
MF	Multiferroic
PZ	Piezoelectric
SEM	Scanning Electron Microscope
TC	Curie Temperature
TN	Neel Temperature
XRD	X-Ray Diffraction
Z	Impedance
Z′	Real Part of Impedance
Z″	Imaginary Part of Impedance

List of Figures

List of Tables

Abstract

Bismuth ferrite ($BiFeO_3$) is a lead free multiferroic, shows both ferroelectric and ferromagnetic properties in single phase a room temperature and has various applications like sensors, actuators, non-volatile memory storage devices etc. In this work, Cu and Ti co-doped bismuth ferrite was prepared via Solid State Mix Oxide Method. Room temperature XRD indexed to the BFO rhombohedral cell with the peak shift towards low diffraction angle representing increase in lattice parameter. Increase in density and decrease in grain size by increasing Cu contents was observed by SEM analysis. The different chemical bonds present in the Ti and Cu doped samples has been identified and confirmed through Fourier Transform Infrared spectroscopy. The complex impedance and modulus have been studied as function of frequency from 100Hz- 1MHz at temperature ranging from room temperature to 250℃ using LCR. The CIS data reveals that magnitude of impedance decreases with rise of temperature and frequency showing NTCR behaviour.

Chapter 1

Introduction

1.1 Introduction

Multiferroics are those materials that incorporate coinciding effects of two or more ferroic properties in same material [1, 2] . The simultaneous existence of two or more order parameters shows infrequent physical phenomena, showing much potential for advanced device utilities [3].

H. Schmid introduced this terminology multiferroic in 1994. This unique definition stated that multiferroics are single phase materials possessing more than two ferroic properties simultaneously. [4, 5]

These ferroic properties are:

- Ferroelectric (FE)
- Ferromagnetic (FM)
- Ferroelastic (FE)
- Ferrotoroidic (FT)

The couplings between these order parameters are:

Magnetoelectricity defines the effect on polarization or magnetization when magnetic or electric field is applied.

Piezoelectricity defines the effect on strain when electric field is applied or effect on polarization when stress applied.

Piezomagnetism defines the effect on strain when magnetic field applied or effect on magnetization when stress applied.

Electrostriction defines the effect on strain when electric field applied as a quadratic function [4]

In recent scientific and researched areas, multiferroic materials are of remarkable significances because they have a potential to be used for sensors, actuators, non-volatile memory storage devices. [4, 6]The magnetoelectrics have engrossed unusual scientific concern because of their unusual physical properties. The assemblage of ferroelectricity and ferromagnetism also makes materials capable for devices which are multifunctional, and the magnetoelectricity offer additional grade of liberty in scheme of advanced devices for example tuneable microwave inactive modules.[7]

In the 19th century, electricity and magnetism were joined into one concept. The concept of combination of magnetic and electric field in insulators is associated with the Pierre Curie. Nevertheless, the actual establishment of this pitch started in 1959 with a petite statement by “Landau & Lifshitz” [6].

The first work devoted to the multiferroics was done by Astrov, who experimentally demonstrated the presence of the magnetoelectric effect in the chromium (III) oxide and studied this effect. Since that, many single-phase multiferroics have been discovered, which includes $BiFeO_3$, $HoMnO_3$, $TbMn_2O_5$, $DyMnO_3$, $LuFe_2O_4$, $Ni_3V_2O_8$, $MnWO_4$, etc. [8]

Table 1.1: History of Multiferroic Materials [9]

Year	Discovery
1894:	Pierre Curie first supposed the magneto electric effect.
1956:	The symmetry necessities for ME effect was expressed by Landau/Lifshitz
1959:	ME effect in Cr_2O_3 analyze by Dzyaloshinskii
1960:	Astrov (ME) authorized experiments
1961:	Rado et al analyze Reciprocal (ME)H effect
1963:	Smolenskii/Kiselev: $BiFeO_3$
1963:	Bertaut et al.: hexagonal $RMnO_3$ (e.g. $YMnO_3$, $HoMnO_3$)
1966:	Ascher/Schmid: Boracites $M_3B_7O_{13}X$ (e.g. $Ni_3B_7O_{13}I$)
1968:	Eibschuetz/Guggenheim et al.: $BaMF_4$ (e.g. $BaMnF_4$ $BaNiF_4$)

The definition has extended to comprise additional orders, e.g. antiferromagnetic. The research field was native in 50's in this broad definition. The related studies have begun from then under the name Magnetoelectric. [5]

The ferromagnetic and ferroelectric are not only the combination of ferroic properties in Magnetoelectric, it is also in any material which are magnetically and electrically polarized, that contains FM, AFM, and PM and AFE and PE.[7]

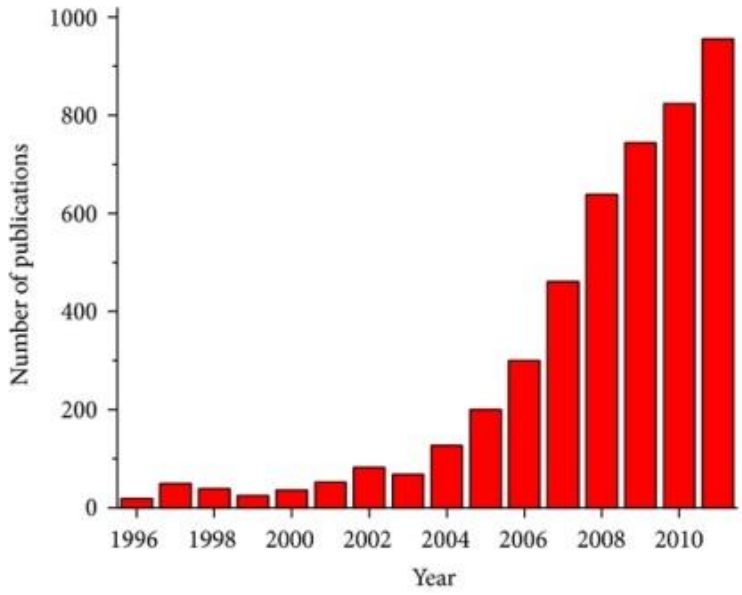

Fig. 1.1: The publications using the keywords Magnetoelectric and Multiferroic

Bismuth Ferrite is multiferroic of single phase which have Curie temperature (Tc=830 °C) and Néel temperature (TN =370 °C) which creates the material suitable for the applications of magnetoelectric. For this resolution, the broad research on BFO bulk and thin film has started which includes its structure and properties. [10-12]

$BiFeO_3$ is the only single phase multiferroic till now that shows FE, AFM and FE orders at room temperature [13]. Moreover, BFO thin films has high remnant polarization and net magnetization associated with a great PE coefficient [14, 15]. These entire properties make a great potential for this material for everyday applications, for example sensors, MEMS and information storage device [16, 17]. BFO bulk has very low polarization but the strong multiferroic behaviour have appealed noteworthy attention in BFO thin film accompanied with high magnetization and polarization, stated in 2003 [18].

A serious problem of epitaxial BFO, i.e. a high value of current leakage at 25°C, is utterly eliminating the polarization and linked FE properties [15,19, 20].

The key problem restrictive applications of Bismuth ferrite is the high value of current leakage initiated by co-occurrence of iron ions (Fe^{3+}, Fe^{2+}), the consequence of oxygen vacancies charge reparation [21-23]. The chemistry of defect theory stated as Bismuth Ferrite doping with valent ions must alter the Fe oxidation state and O^{2+} vacancy concentration, making means for controlling the Bismuth Ferrite current leakage. [7]

Such kind of problems hinders the electrical and magnetic properties of ceramics. Since these materials are treated on high temperature so the defects cannot be avoided [24]. To obtain mandatory properties and to draft microstructure it is very important to study such influences, which comprises of the existence of defects, concentration of defects, chemical variation, preparation environments & procedures and temperature range of analysis. [25]

The high temperature electrical and magnetic properties of Bismuth Ferrite with varying doping elements and concentration are not being studying commonly because of its defects. The objective of presented work is to study the effect of doping on the properties of $BiFeO_3$, effect of CuO as a sintering aid and Ti to increase multiferroic properties, added as dopants in Bismuth Ferrite and to study the relationship between microstructural and multiferroic properties of BFO ceramics.

Chapter 2

Literature review

2.1. Multiferroics

Multiferroic materials which show more than one or two order parameters all together; FE, FM, and FE order, display uncommon combination of properties, and ability of advanced applications in devices. Fig.2.1 illustrate the phase control in various types of couplings exists in the system. The E, H, and σ (electric, magnetic field and stress) govern the P, M, and ε, (polarization, magnetization and strain) [26].

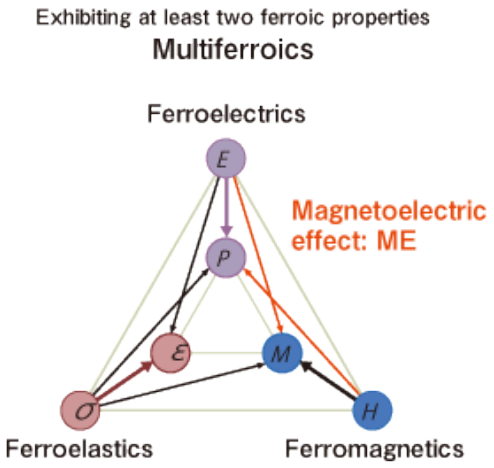

Fig. 2.1: Phase control in ferroic and multiferroic

Ferroelectricity: electric polarization induced spontaneously in a material that might be upturned due the influence of electrical field applied externally.

Ferromagnetism: spontaneous magnetization below the critical temperature.

Ferroelasticity is a disclosing of an impulsive strain in a material. A phase change occurs of different crystal structure, when stress is applied to material (e.g. cubic to tetragonal) [27].

Multiferroics have several crystal arrangements. There are four main groups that allocate the multiferroic by Smolenskii & Chupis [28] .

- **Perovskite (ABO_3) Structure**, materials which have B position fully or partly occupies by magnetic ions. This is the major class, and the follower of this class is BFO. This class also contains layered compound with complex perovskite type structure of $A_{m+1}B_mO_{3m+3}$ formula where A= Bismuth, Calcium and B= Iron, Titanium.

- **Hexagonal-structure rare-earth manganite $RMnO_3$,** where R= rare earth metals have high FE with AFM or FM properties. $YMnO_3$ is the most considered participant of this family.

- **Boracites**, $M_3B_7O_{13}X$, where M = Chromium, Manganese Iron and X= Halogens, and they are FE and AFM or low FM.

- **Compounds with a general formula $BaMF_4$**, where M=Manganese, Iron, Cobalt. This family shows FE properties with AFM or low FM at room temperatures.

2.2. Ferroelectricity

FE is from broader group known as pyroelectrics, which are from the class of PE. Pyroelectricity defines as ability to generate charge within some materials which is effect of varying temperature, and PE defines as the effect on electric potential when stress applied. All pyroelectric systems also have PE, however not in reverse, for example quartz. The FE possesses PE & pyroelectricity, but FE are not PE. For example, the materials have band gap wide e.g. Gallium Nitrate, Aluminium Nitrate, and Zinc Oxide are not FE while both are pyroelectric and PE.

FE are class of materials display polarization which induced spontaneously at temperature lower than TC, and when the electrical field applied the direction of polarization can be altered. Above the Curie temperature, all the materials become non-polar and no more FE behave normally as dielectrics. Mostly, there can be TC more than one, while the most FE possesses one TC. There may also FE material, which does not show TC for the reason that the material commences decaying, prior to TC [7].

2.2.1. Ferroelectric Materials and their Crystal Structures

The most commonly considered and used FE has ABO_3 type structures which possess typical cubical lattice symmetry at high temperature. The cubical perovskite lattice symmetry is considered to be cation “B” of smaller size at centre of oxygen anions of octahedron, with cation “A” of larger size at the corners of unit cell. Temperature below the TC, a distortion of structure from higher symmetry form to lower symmetry form arises. This distortion corporates by a shift of smaller cation from off-centre, which is the most important feature giving growth to the spontaneous polarization [29].

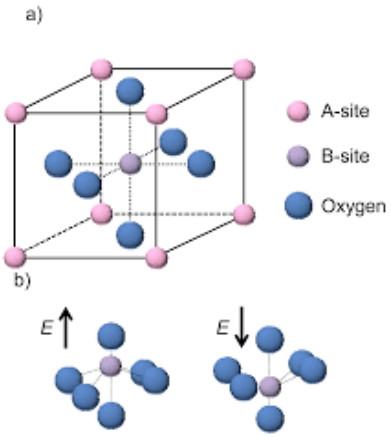

Fig. 2.3: The perovskite structure (a) the cubic phase,

(b) Dipole swapping when electric field is applied.

Ferroelectricity is produced by few different mechanisms:

- Ferroelectricity in multiferroic perovskites, the transition metal ion shifts from off-center is origin of ferroelectricity. These ions are strongly bonded covalently with one or even more than two O^{2+}, by its vacant "d" shell. Though, the theory for this situation has not yet been made clear.

- Ferroelectricity created by active lone pair cations, for example Bismuth or lead in $BiFeO_3$ or $PbVO_3$

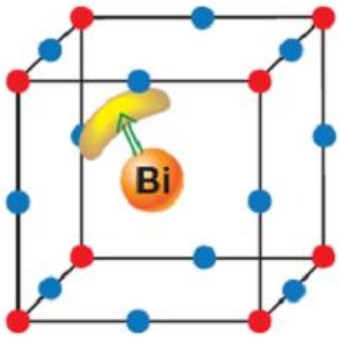

Fig. 2.4: In $BiFeO_3$, Bi^{3+} ions (orange) are contributing

To polarization (green arrow) has lone pairs

Ordering (yellow lobes)

2.2.3. Spontaneous Polarization

The FE materials contain **domains**, (regions which are uniformly polarized spontaneously). The separation of neighbouring domains is known as **domain wall**. When the electrical field is absent, the domains are aligned arbitrarily, which polarized the material. With the applying of electric field, field aligned the domains lengthwise, initiating the polarization in material. Domain alignment starts switching and it moves along the boundary of domain. The DE, PE and FE properties are involved by domain and domain dynamics are known by means of important device applications in FE, hence the scientist research has great interest on these applications [30, 31].

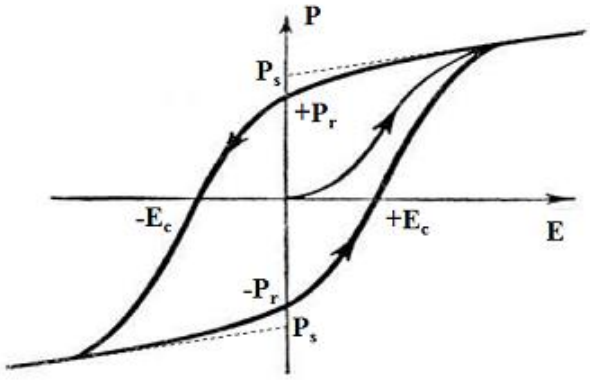

Fig. 2.5 Hysteresis curve of FE (P-E).

Reversibility of permanent polarization is the important characteristics of FE materials, which depend upon the polarization on electrical field similar to magnetization curve in FM material, results in hysteresis curve. The hysteresis curve is considered to have *Ps*, *Pr*, and *Ec*. The diagram is shown in the fig. 2.4

Saturation polarization defines the highest value of polarization that a material can attain.

Polarization defines as the material's polarization in the absence of electrical filed.

Coercive field defines as the value at which zero polarization that an electric filed can bring.

The domain structure of the ferroelectric is the result of P-E hysteresis loop which completed at the temperature lower than TC which is exertion to get the value of depolarization field minimum. The unique characteristics of FE are:

- Spontaneous polarization at lower than TC.
- The nonlinear polarization depends upon electric field.
- Occurrences of structures of domain at lower than TC.
- The value of DE constant is high (upto 2x104).
- High values of PE and pyroelectric constants [7].

Table 2.1: The FE materials with their pertinent properties [27, 32-34].

Compound	**Chemical formula**	**Year discovered**	**Symmetry at room temp.**	**Curie point, T_c, K**	**Remanent polarization, P_s, μ*K·cm***
Rochelle salt	$KNaC_4H_4O_6 \cdot 4H_2O$	1921	Orthorhombic	297	0.25
Barium titanate	$BaTiO_3$	1945	tetragonal	398	25
Lead titanate	PbTiO	1950	tetragonal	763	20-96.5
Lead zirconate	$PbZrO_3$	1951	Orthorhombic	503	20-50
Bismute titanate	$Bi_4Ti_3O_{12}$	1961	Orthorhombic	953	10-30

2.3. Ferromagnetism

FM defines as the phenomenon due to which some of the materials for example Fe becomes permanent magnet or is attracted towards magnet.

Ferromagnetism was discovered more than 2000 years ago. Ferromagnetic materials experience a change from a paramagnetic at higher temperature to phase exists at lower temperature which holds spontaneous and nonvolatile magnetization, below some phase transition temperature called the Curie temperature (Tc)

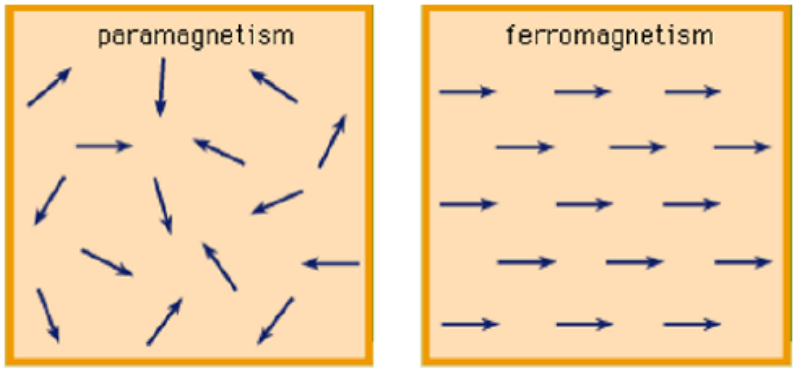

Fig. 2.6: Magnetic ordering in ferromagnetism

The basis of the magnetism is because of the localized electrons, from the “d” or “f” shells of transition metal or rare-earth metals. These shells are partially filled with the own spin or magnetic moment possessed by electrons. Localized moments lead to magnetic order by exchanging interfaces. Long range order in ferromagnetic material shows that spins of electrons which are unpaired in a region become line up, parallel with each other. The region is called a domain as shown in fig. 2.6. However, ferromagnetic materials often have no macroscopic magnetization because their magnetic domains are aligned in different directions.

Moments throughout a material in 3-D tend to oriented parallel can cause a spontaneous permanent M (in absence of H) but, in a macroscopic system, it is promising for spins to segregate into regions called **Domains**. Domains need not be oriented with each other, may or may not possess spontaneous M application of H creating aligned domains to rise at the cost of misaligned domains alignment continues when H is removed. Ferromagnetism is a critical mechanism, including a phase transition that arises at a critical temperature, Tc = Curie temperature. Above Tc → paramagnet[35]

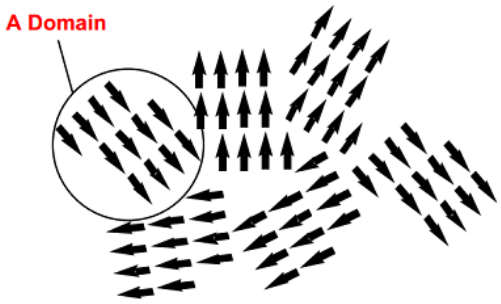

Fig. 2.8: Domains in ferromagnetic materials

There are two theories of ferromagnetism that describe FM several properties:

1. The theory of Curie-Weiss localized moment

2. The theory of Stoner band of ferromagnetism

2.3.1. The Curie-Weiss localized-moment theory

According to Weiss’s theory, electrons are localized, conquering certain energy levels. The energy of an electron is influenced by its angular momentum. The core molecular field oriented the electron’s magnetic moments. These orientations are parallel to each other

in magnetic moments. The field of this molecular orientation initiates from the quantum mechanical exchange energy.

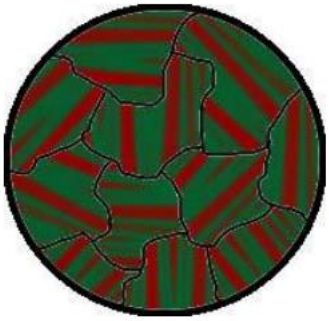

Fig. 2.9: Weiss Domain structure

2.3.2. The Stoner band theory of ferromagnetism

According to Stoner theory, electrons are allowed to change in a periodic potential. If all electrons have the same spin, the exchange energy is reduced [29].

Table 2.2: Multiferroic materials along with their physical properties [10, 28, 36-58]

Multiferroics	Space group	Crystal structure	Magnetic ordering	Electrical ordering	$T_{N,M}$, K	T_C, K
$YMnO_3$	$P6_3cm$	hexagonal	AFM	FE	70 -80	914
$YbMnO_3$	$P6_3cm$	hexagonal	AFM	FE	87	983-993
$HoMnO_3$	$P6_3cm$	hexagonal	AFM	FE	72 (~49[819])	875
$TmMnO_3$	$P6_3cm$	hexagonal	AFM	FE	86	>573 (348[821])
$TbMnO_3$	Pbnm	orthorombic	AFM	FE	41	28
$DyMnO_3$	Pbnm	orthorombic	AFM	FE	~40	~19
$LaMnO_3$	Pbnm	orthorombic	AFM		140	
$BiMnO_3$	C2	monoclinic	FM	AFE	105	723
$BiFeO_3$	R3c	rhombohedral	AFM	FE	643	1100
$BiCrO_3$	C2/c	monoclinic	AFM	AFE	109	420
$HoMn_2O_5$	Pbam	orthorombic	AFM	FE	~45	~39
$ErMn_2O_5$	Pbam	orthorombic	AFM	FE	~45	~39
$TmMn_2O_5$	Pbam	orthorombic	AFM	FE	~45	~36
$TbMn_2O_5$	Pbam	orthorombic	AFM	FE	~45	~38
$DyMn_2O_5$	Pbam	orthorombic	AFM	FE	~42	~38
YMn_2O_5	Pbam	orthorombic	AFM	FE	~45	~41
$BiMn_2O_5$	Pbam	orthorombic	AFM	FE	39	~38
$Ni_3B_7O_{13}I$	$F\bar{4}3c$ (77 K) $Pca2_1$ (<62K)	cubic orthorhombic	AFM	FE	~120	<64
$Ba_{0.5}Sr_{1.5}Zn_2Fe_{12}O_{22}$	$R\bar{3}m$	hexagonal	noncollinear helical spin structure	FE under applied magnetic field	326	~130
Bi_2FeCrO_6	R3	rhombohedral	ferrimagnetic		between 600 and 800	above RT

2.4. Bismuth Ferrite ($BiFeO_3$)

BFO is the first considered multiferroics with the perovskite structure. It was also studied that it has remarkable FE which has TC= 850℃ and AFM has TN=370℃ ordering temperatures (TC is Curie temperature, TN is the Neel temperature), but the highest value of the polarization (P) in the single-crystal $BiFeO_3$ found to be very small (3 ± 6 mC/cm^2).

In inconsistency to the single crystals, the extents of the pyroelectric current in the thin epitaxial films of bismuth ferrite have exposed to be high polarizability, attaining values of 60 ± 100mC/cm^2. The main purpose for such small polarization in the before investigation bulk crystals is the leakage current instigated by nonstoichiometry and imperfections, which was removed in the thin film state and later in the high quality single and polycrystals17 ± 19mC/cm^2.

The processing of the $BiFeO_3$ phase is complex, on one hand, by high possibility of the development of impurity phases such as sillenite $Bi_{25}Fe_xO_{20}$ (isostructural to the meta-stable g-Bi_2O_3) and $Bi_2Fe_4O_9$ at the grain boundaries of polycrystalline ceramics and, on the other hand, by the strong reliance on the crystal perfection and oxygen stoichiometry of the physical properties. Low leakage currents and the presence of magnetic moment in the crystal both are essential for the useful application of bismuth ferrite; hence, special considerations have given to enhancement of FE characteristics and cycloidal AFM order annihilation in $BiFeO_3$. The native spin structure in bismuth ferrite is of G-type AFM in which every Fe^{3+} ion surrounds by 6 Fe^{3+} ions and have opposite spin movement. [8].

2.4.1. Structure and Properties of $BiFeO_3$:

The perovskite Bismuth Ferrite was discovered in the 1959. Bismuth Ferrite is recognized as antiferromagnetic, ferroelectric multi-ferroic with an AFM Neel temperature of TN=370℃ and FE Curie temperature of TC= 850℃ in its bulk form. Bismuth Ferrite adopts structure of perovskite type and not the ferrite structure, irrespective of its nomenclature.

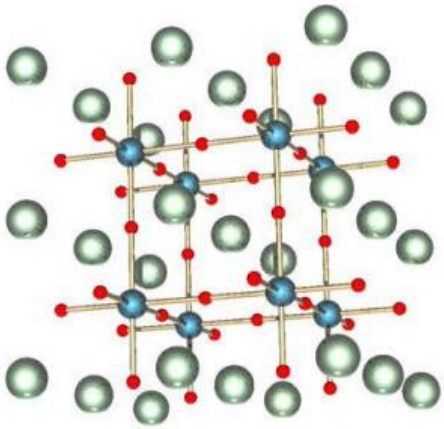

Fig. 2.10: Perovskite structure of ABX_3 chemical formula

The X atoms are in red spheres usually oxygen, the B-atoms

Are in blue spheres and the green spheres is A atom

Bulk bismuth ferrite can be well-defined as a rhombohedral ferroelectric with distorted perovskite structure and space group R3c as shown in figure 2.11. The rhombohedral unit cell has a = 5.59 Å and α = 60.68° lattice parameters. The perovskite distorted structures of R_3c space group have growth of spontaneous polarization along the direction of [111] of psuedocubic. In Figure 2.11, the hexagonal representation of Bismuth Ferrite unit cell is shown. On the other hand, an illustration is used which is pseudocubic, in which [001] hexagonal is equivalent to [111] cubic. At face-centred sites the oxygen atoms are present of the Bismuth cubic structure. BFO ceramics are revealed to be FE having polarization along the direction of rhombohedral c-axis. This is due to the dislocation of Bismuth and Iron, Oxygen comparative to each other.[59]

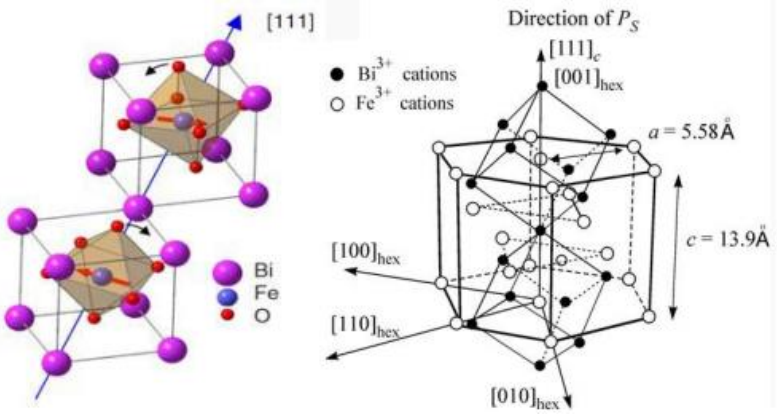

Fig. 2.11: Crystal structure of bulk $BiFeO_3$

2.4.2. Effects of A and B Sites Substitution in BFO Structure

The BFO has large value of leakage current density which initiate from various factor such as impurity phases and poor microstructures, volatilization of Bismuth ions, oxygen vacancies and valence fluctuation of Fe^{3+} ions (Fe^{2+} /Fe^{3+}). Various Studies are continuing to resist the density of leakage current. To enhance the FE properties of the Bismuth Ferrite different techniques are used, which include,

- Creating resistive buffer layers.
- Single crystal substrates.
- Creating solid solutions.
- Manufacturing a multilayer structure.
- Cationic replacement.

Substitution in $BiFeO_3$ of impurities which includes rare earth metals at Bi site and transition metals at Fe-sites is the most suggested method to enhance the FE properties and to control the large density of leakage current. The perovskite structure becomes steady with the doping of rare earth ions at Bi-sites. It controls the vaporization of Bismuth ions and maintains the non-Centro symmetry. The substitution of transition metal ions at Fe-sites in BFO system fills the oxygen vacancies based on the valence compensation and reduce the valence fluctuation of Fe^{3+} ions [58, 60].

Recent researches on Bismuth Ferrite have developed some electrifying scientific consequences to enhance its FE and FM properties by inclusion of impurities at Bismuth site (A-site). Some research resulted that this type of impurity inclusion at A or B site results in improvement of the multi-ferric properties of the system. But in some cases, the magnetic properties can be enhanced by the existence of a valance state of 2+ of Fe separated from the expected 3+ valance state. Also, magnetic properties can be increased by keeping particle size of less than 62nm, increased Fe-O-Fe canting and homogenization of spin structure. [61].

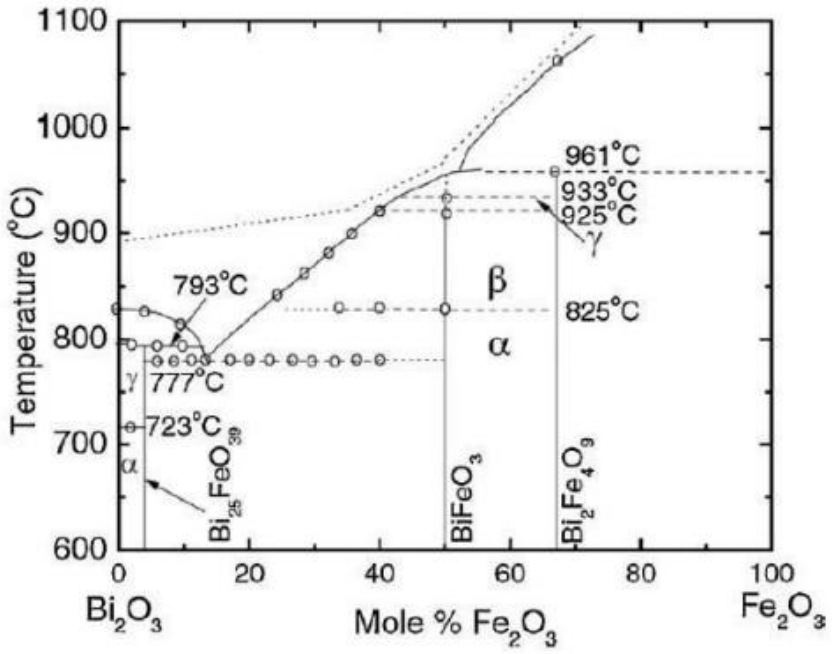

Fig. 2.12: Phase Diagram of Bismuth ferrite

2.5. Effect of Dopants

i. Effect of Neodymium (Nd) and Cobalt (Co):

There co-doping of Nd and Co have many effects. The solid state mixed-oxide method is used to prepare the substitution. The density of the ceramic increases and grain size decreasing as the co-doping concentration increases. The increase in co-doping concentration increase the remanent magnetization while the coercive magnetic field reduced [62]

ii. Effect of Manganese:

The spontaneous magnetization with the precision of magnetic hysteresis is increased by the increase of Manganese doping concentration. The increase in magnetization is understood by the alteration of the spiral G-type AFM to a collinear G-type AFM ordering. In this alteration, anti- ferromagnetically ordered spins canted component becomes firm for the magnetic structure[63].

iii. Effect of Strontium

The magnetic properties of BiFeO3 have been improved by the chemical operation. The important purpose of MF material is to create magnetic order strong coupling at room temperature. This can be attained by substitutions at both Sites A and B. The B-site Sr doping

resulted in being oxygen sub-stoichiometric. When the Sr concentration increases, a transition occurs to the $SrFeO_3$ phase which results in decreasing magnetization of system.

iv. Effect of Barium (Ba) and Calcium (Ca)

Barium substituted BiFeO3 possessed ferromagnetism and ferroelectricity simultaneously. Ca doped bismuth ferrite material exhibits coupling of ferromagnetism and ferroelectricity.

v. Effect of Copper (Cu)

The result of addition of Cu to Bismuth ferrite, the density and the electrical properties enhanced. Owing to Cu doping, dielectric constant increases and the dielectric loss which is also known as loss tangent minimized. Cu acts as a sintering aid for $BiFeO_3$[64]

vi. Effect of Titanium (Ti)

The magnetic and electric properties are enhanced by co-doping of BFO with Ti. The remanent magnetization rises by the substitution of Ti to BFO. The Partial destruction of spin cycloid by co-doping of $BiFeO_3$ and structural distortion makes the magnetization grow. Moreover, there is a dielectric loss due to substitution of Ti in BFO[65].

2.6. Applications of Bismuth Ferrite ($BiFeO_3$)

Some of the applications of $BieO_3$ are listed below:

- Spintronics and Magnetoelectric Access Memory MERAM
- BFO's emission of THz radiation
- Potential and memory devices
- Spin Valve Structure

Chapter 3

Experimentation

3.1 Experimentation

This chapter briefly describe the experimental procedure carried out and the characterization techniques used to achieve the objective of the research. The experimental method describes the doping Bismuth Ferrite $BiFeO_3$ with Copper Cu and Titanium Ti of different amount followed by the brief description of characterization techniques used to characterize the properties of samples. It includes Scanning Electron Microscopy, X-Ray Diffraction, Fourier Transform infrared Spectroscopy and Complex Impedance Spectroscopy.

3.2. Experimental Procedure

Bismuth ferrite co-doped with Titanium Ti and Copper Cu was prepared via solid state method. Bi_2O_3, Fe_2O_3, TiO_2, CuO were added with stoichiometric amount as indicated in table. Bismuth ferrite co-doped with Ti and Cu in which Ti is fixed and effect of varying amount of Cu has been studied.

- Raw materials were pre weighed in electronic balance using stoichiometric amounts according to the stoichiometric composition
- They were mixed in ball mill for five hours using zirconia balls with solvent ethanol in Teflon pots to reduce particle size and uniform mixing to get uniform phase during calcination.
- After mixing, powder was dried in oven at 60°C. After mixing, powder calcination was done at 800°C for one hour in muffle furnace to get homogeneous phase and require calcined product
- After calcination sample was again mixed/crushed for half hour using pestle and mortar. Samples were then pressed in hydraulic press machine (load/pressure = 2000 pounds, dwell time = 40 sec). Pellets of 10mm diameter were prepared
- These pellets were sintered at 830°C for two hours to get maximum densification. After sintering these samples were used for characterization.
- Density of these pellets was measured by using conventional method.
- X-ray diffraction technique used to analyze crystal structure.
- Scanning electron microscope used to study the microstructural analysis.
- Fourier transforms infrared spectroscopy used to identify the chemical bonds.
- Complex impedance spectroscopy used to study the electrical response of the samples.

3.2.1 Stoichiometric Calculations for 10g Sample

Table 3.1: Stoichiometric Calculations

No. of Compositions	Chemical Formula	Bi_2O_3 (g)	Fe_2O_3 (g)	CuO (g)	TiO_2 (g)
1.	$BiFe_{0.867}Cu_0Ti_{0.1}O_3$	7.513	2.23	0	0.257
2.	$BiFe_{0.856}Cu_{0.015}Ti_{0.1}O_3$	7.506	2.200	0.038	0.257
3.	$BiFe_{0.85}Cu_{0.025}Ti_{0.1}O_3$	7.497	2.182	0.064	0.257

3.3. Characterization Techniques

The crystalline structure, elemental analysis and electrical properties of material are analysed by using different characterization tools, which are:

- X-Ray Diffraction.
- Scanning Electron Microscopy.
- Fourier Transform Infrared Spectroscopy.
- Complex Impedance Spectroscopy

3.3.1. X-Ray Diffraction Analysis

3.3.1.1 Scope

X-rays are radiations of electromagnetic having wavelength 1Å (10-10 m). This is the same as an atom is size of. XRD give most complete information of structure, distance between atoms and angles between bonds. XRD is used to study the properties of metals, alloys, polymers, minerals, amorphous materials inorganic and organic compounds. X-ray diffraction analysis is most successful method to study crystalline structure because crystals are arranged in periodic manner of atoms and constitute which naturally produced diffraction gratings for X-ray.

3.3.1.2. Working

XRD is used to classify the structure of atoms and molecule of a crystal. The x-ray beam diffract from many crystalline atoms. The angles and intensities of these diffracted beams are determined. This determination creates a 3-D picture of the electrons density which are in the crystal. The mean atomic positions in the crystal, chemical bonds, their disorder and some other properties can be determined by the electron density.

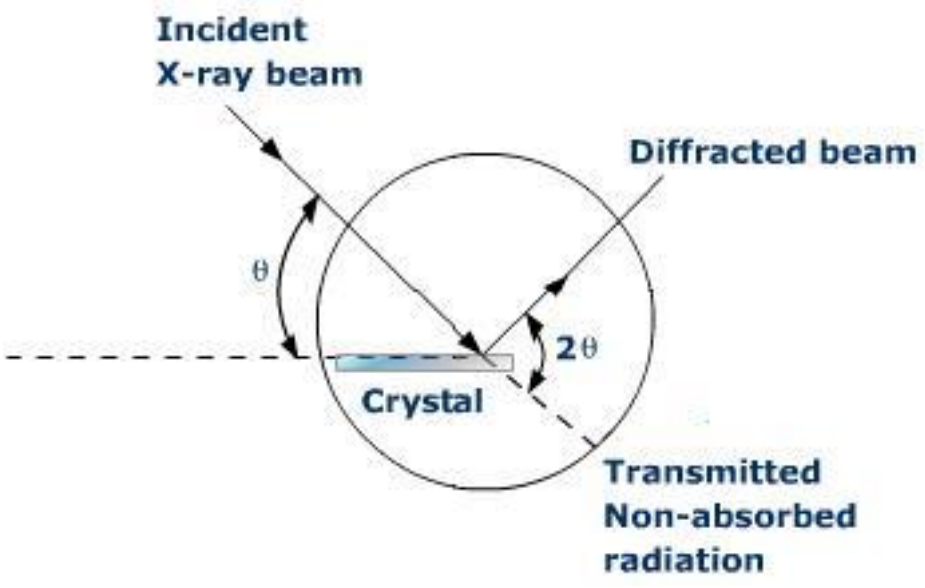

Fig. 3.1: X-Ray Diffraction illustration

3.3.2 Scanning Electron Microscope (SEM)

3.3.2.1 Scope

The Scanning electron microscope uses EDS to create the elemental maps. These elemental maps exactly signify the elemental distribution within samples. It is commonly use in contrast, elemental analysis, morphology, and mineral orientation. The Scanning electron microscope is compressed in power through newly invented microscopes. The SEM is very valuable on the market but other microscope can also work with a equally wide sample range.

3.3.2.2 Image Formation Process

In Scanning electron microscope, electron gun is used to discharge electron thermionically. Filament of Tungsten is used to create electrons. Due to highest melting point and lowest vapour pressure of all metals filament is used in electron gun thermionically.

The beams of electrons have energy from 0.2 keV to 40 keV. The beam is focused by more than one condenser lenses directed towards a point which has diameter 0.4 nm to 5 nm. The beam of electron passes by pairs of coils or deflector in the electron column usually in the final lens. These lens bounce the beam on the x and y axis and image is created in a faster manner at area of the sample surface rectangular in shape. The electron beam and the sample contact produces reflection of high-energy electrons. The beam current which is captivated by the sample can also be perceived. The beam current can be used to make images of the dispersal of specimen current [66].

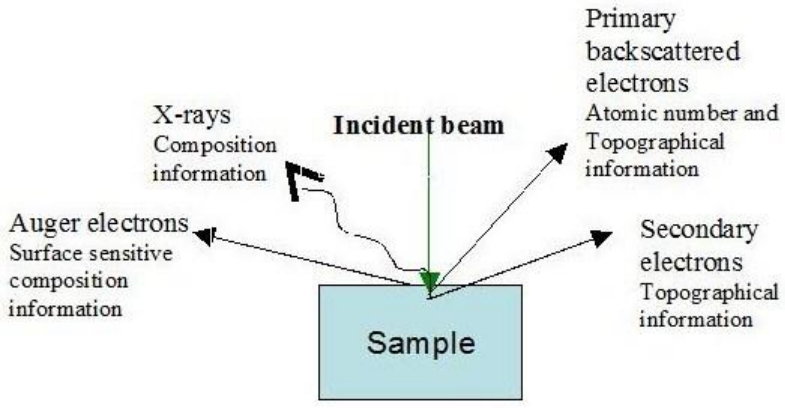

Fig.3.2: Scanning Electron Microscope diagram

3.3.3 Fourier Transform Infrared spectroscopy

FTIR spectroscopy is technique, used for material investigation, of non-destructive class. FTIR is the study of infrared radiation interacting with matter in terms of frequency of photon. FTIR offers precise data of the vibration and bending of the molecular structure and chemical bonding. This information makes data suitable to analyse certain inorganic materials and organic materials.

The FTIR spectra show absorption peaks that are linked to the frequencies of vibrations between the bonds of the atoms creating up the material called fingerprint frequency. The absorption peaks obtained at higher frequency showing stretching between the bonds called group frequency. The Bending absorption is smaller than stretching peaks because less energy required stretching the bond than to bend the bond. The bending vibrations range from 10-1600 cm^{-1} and stretching vibration 1600-4000cm^{-1}. The size of the absorption peaks in the spectrum is signal of the amount present in the material.[67]

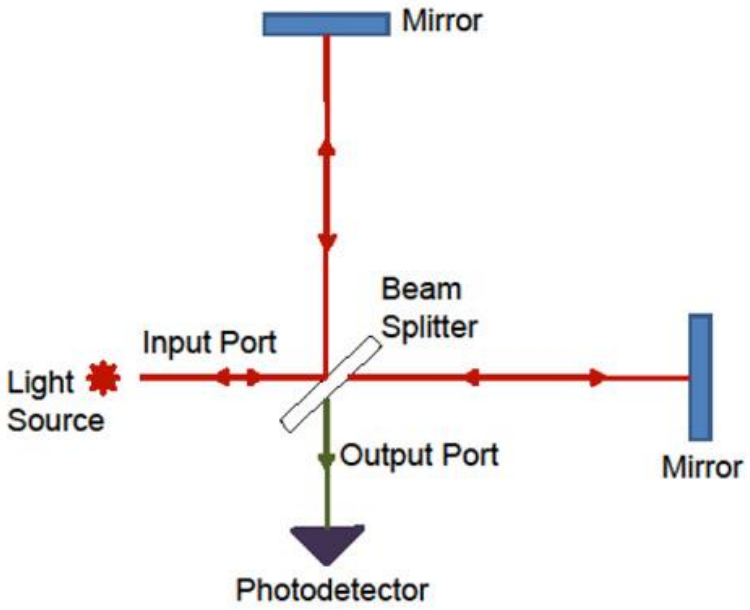

Fig.3.3: Schematic Diagram of FTIR

3.3.4 Complex Impedance Spectroscopy

CIS is a moderately operative technique to study the electrical properties of materials. This technique gives a significant instrument to create contact between electrical properties of material and microstructures. This method consists of applying AC signal across the pellets of specimen and then measuring the productive response. The ceramics are comprised of two areas called grain and grain boundary. These both areas are differing from one another in physical properties.

The study of CIS data can rather be obtained by consuming the equivalent circuit which consists of two parallel combinations of R and C or connected in series with each other in a circuit. [68]

Relative Permittivity $\varepsilon^* = \varepsilon' - j\,\varepsilon''$

Impedance $Z^* = Z' + j\,Z'' = 1/\,j\omega Co\,\varepsilon^*$

Electric Modulus $M^* = M' + jM'' = 1/\,\varepsilon^*$;

Admittance $Y^* = Y' + jY'' = j\omega Co\,\varepsilon^*$

And $\text{Tan}\delta = \varepsilon''/\,\varepsilon' = M''/M' = Z'/\,Z'' = Y''/Y'$,

Where,

f= frequency; $\omega = 2\pi f$ is the Angular Frequency

$Co = \varepsilon o\, A/t$ is the geometrical Capacitance

$j = \sqrt{-1}$; εo is the Permittivity of Vacuum (8.854×10^{-12} F/m)

t and A are the thickness and area of the pellet;

and δ is Complementary $(90-\theta)$ to the phase angle (θ).

Chapter 4

Results & Discussion

4.1. X-Ray Diffraction

Room temperature XRD graph of Cu and Ti doped BFO pellets are shown. The XRD graph of $BiFe_{0.867}Cu_0Ti_{0.1}O_3$, $BiFe_{0.856}Cu_{0.015}Ti_{0.1}O_3$, and $BiFe_{0.85}Cu_{0.025}Ti_{0.1}O_3$ are shown in figures 4.1.

The major peaks can be indexed to the $BiFeO_3$ rhombohedral cell. The non-perovskite $Bi_2Fe_4O_9$ secondary phase peaks before 30º were observed in 0%Cu $BiFeO_3$ ceramic. It is familiar that single phase $BiFeO_3$ is quite difficult to synthesize by the standard solid state procedure. The Bi_2O_3 volatility of high value leads to the development of secondary $Bi_2Fe_4O_9$ phase or any other phase. However, when dopants at the Fe sites are added, impurity peaks are inhibited and single phase was found with the entire peaks equivalent to the rhombohedral structure having the R_3c space group. Peak splitting at 2θ 32º, 40º, 53º and 58º shows rhombohedral lattice symmetry. Additionally, Cu ion substitution at Fe-site in BFO is expected to shift peak to lower values of 2θ. This is because of the ionic radius of Cu^{+3} (54pm) smaller than ionic radius of Fe^{+3} (78 pm). The diffraction peaks intensity in the samples drops when Cu concentration rise, which shows that the degree of crystallinity decreases.[69, 70]

This discloses that the Cu ions present in BFO system inhibit the crystal grains growth. To preclude the growth of particle, the grain boundaries motion should be hindered. When the grain boundaries motion attached to the ferric interstitials which are substituted by Cu ions they propose an impeding force on grain boundaries. If this impeding force engendered is more than the grain growth driving force, the grain cannot propagate further.[1]

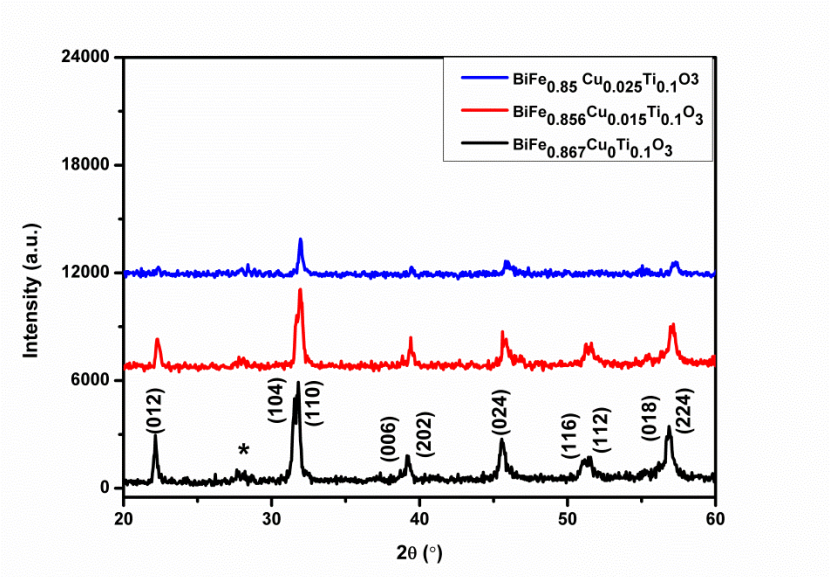

Fig. 4.1: XRD patterns of $BiFe_{0.867}Cu_0Ti_{0.1}O_3$, $BiFe_{0.856}Cu_{0.015}Ti_{0.1}O_3$ and $BiFe_{0.85}Cu_{0.025}Ti_{0.1}O_3$

4.2. Scanning Electron Microscope

The microstructural analysis of Copper and Titanium doped $BiFeO_3$ pellets are studied from SEM. The Scanning electron Microscope images of $BiFe_{0.867}Cu_0Ti_{0.1}O_3$, $BiFe_{0.856}Cu_{0.015}Ti_{0.1}O_3$, and $BiFe_{0.85}Cu_{0.025}Ti_{0.1}O_3$ are shown in figures 4.2.

The $BiFeO_3$ sample has large grain size approx. 10 μm and big voids between the grains are present. These voids are result of Bi_2O_3 volatilization and ensuring oxygen vacancies during processing at elevated temperatures. Co-substitution makes the sample relatively denser with arbitrary shaped grains. Smaller grains are also observed in Cu and Ti doped BFO sample. Fig (a) shows BFO sample with Ti doping have smaller grains with size ranges 1-1.5 micron. In Fig (b, c, d) more reduction in size of grains has been observed as the amount of Cu increases. The average grain size ranges in 0.2- 0.5micron with Cu and Ti doping. The co-substituted samples have reduction in grain size. This reduction is result of the decrease in the oxygen vacancies. The model of space charge stated as the higher concentration of doping elements at the region of grain boundary will make gradient of concentration between the (grain bulk) and grain boundary. Additionally, doping reduces the movement of cations at grain boundary that results in larger density and obstructs the growth of grain. [69]

(a)

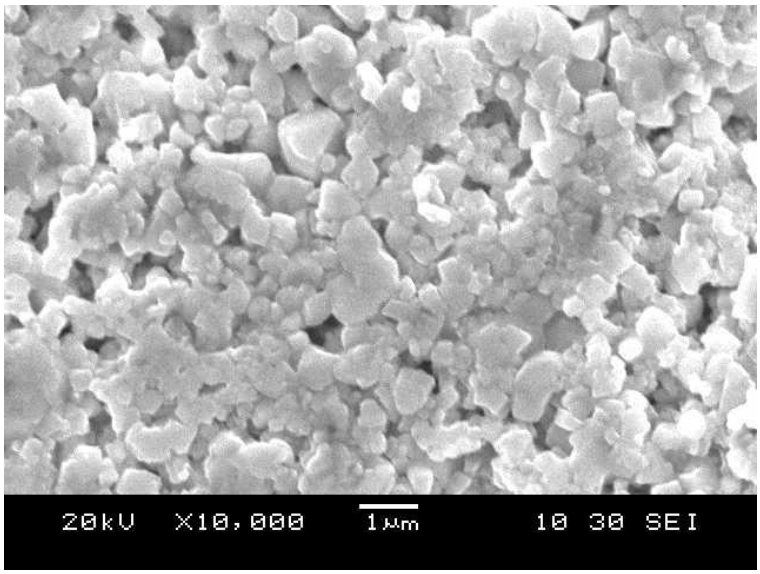

(b)

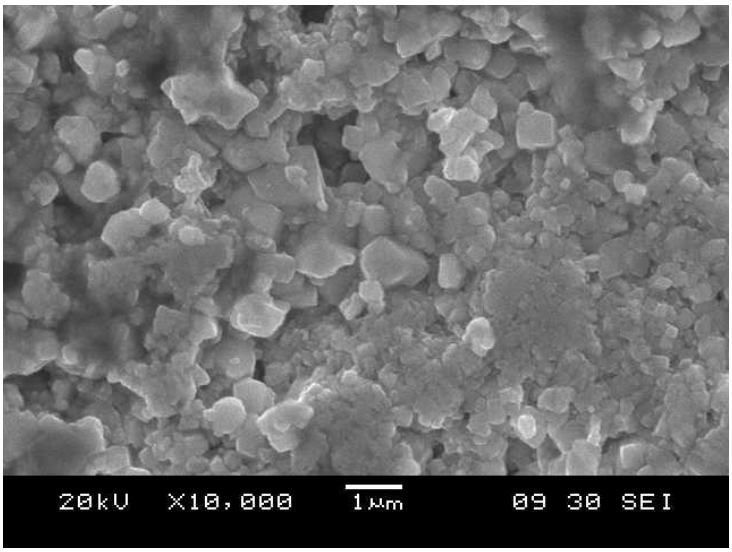

(c)

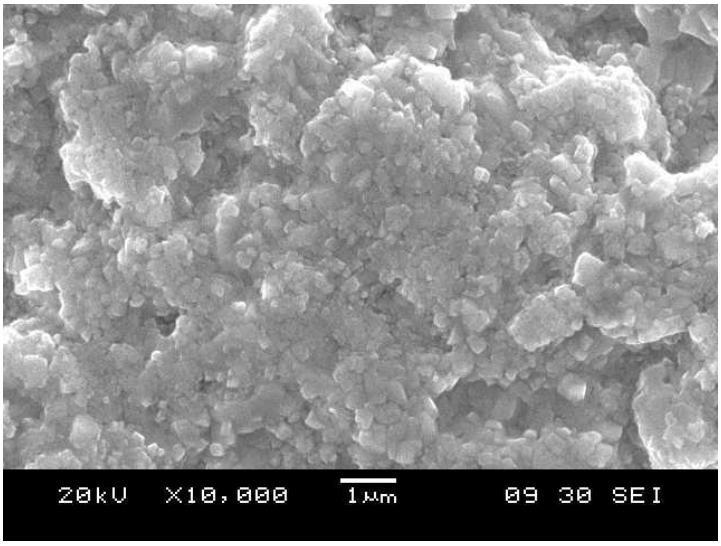

Fig.4.2: SEM images a) $BiFe_{0.867}Cu_{0}Ti_{0.1}O_3$, b) $BiFe_{0.856}Cu_{0.015}Ti_{0.1}O_3$, c) $BiFe_{0.85}Cu_{0.025}Ti_{0.1}O_3$

4.3. Fourier Transform Infrared Spectroscopy

The FTIR spectra of Copper and Titanium doped BFO pellets recorded in wave number range 400–3000 cm^{-1} is shown in figure 4.3. Normally, the vibrations of perovskite type have spectra in this range.

For all the samples, the two strong peaks at 488 cm^{-1} and 508 cm^{-1} have observed. These peaks are characteristic to bending vibrations of O-Fe-O of octahedral FeO_6 groups in perovskite compounds. All the other small peaks obtained in the range of 400–600 cm^{-1} give evidence of the presence of very small amount of carbonaceous. The bands arising at 600-800 cm^{-1} attributed to the vibrations of bending of CuO and oxides of bismuth. The bands arise at around 900cm^{-1} and 1000-1040 cm^{-1} attributed to the traces of trapped NO^{3-} ion and vibration of bending symmetry of C–H bond existing in the sample. [71, 72]

The doping of $BifeO_3$ with Ti and Cu causes change in the bond length, bond angle and coordination number. This alteration in crystal symmetry is accountable for the small shifting of absorption bands in FTIR spectra.[1]

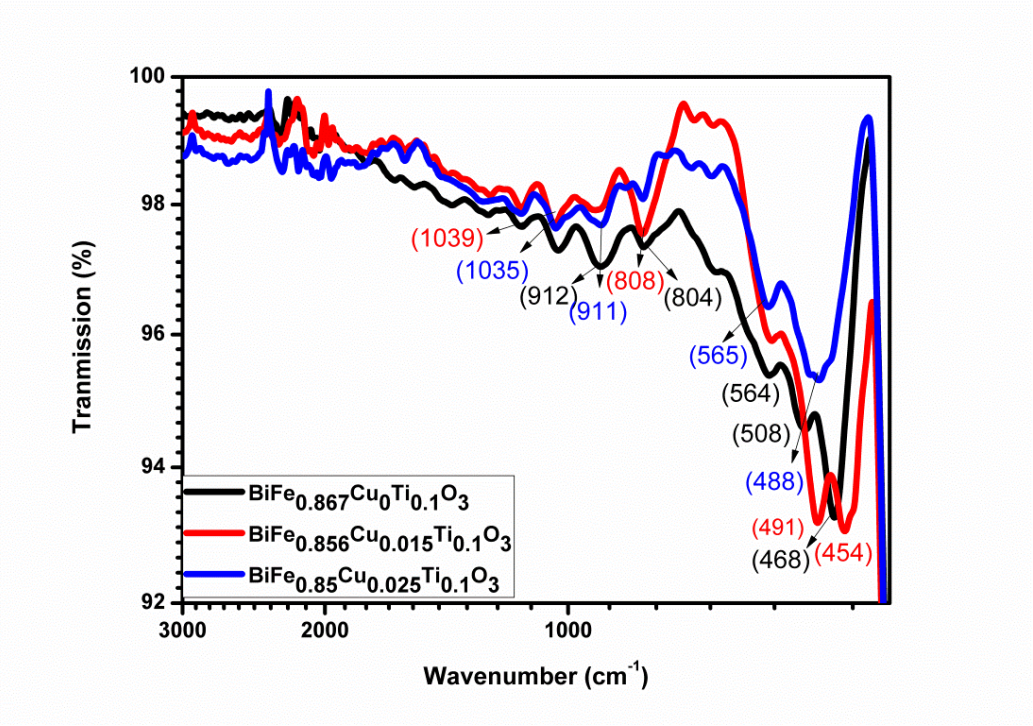

Fig. 4.3: FTIR spectra of $BiFe_{0.867}Cu_0Ti_{i0.1}O_3$, $BiFe_{0.856}Cu_{0.015}Ti_{0.1}O_3$ and $BiFe_{0.85}Cu_{0.025}Ti_{0.1}O_3$

4.4. Complex Impedance Spectroscopy

CIS is a renowned technique to explain the surface, interface, grain/grain boundary properties of polycrystalline electro ceramics. The grain and grain boundary properties, relaxation frequency and electronic conductivity of dielectric materials are better examined by this procedure. The two successive semicircles are obtained from polycrystalline material which shows grain and grain boundary properties with different time constants [70]

Fig. 4.4 shows the plot of real and imaginary part of impedance (Nyquist's diagram) in frequency range of 100Hz- 1MHz at different temperatures of $BiFe_{0.867}Cu_0Ti_{0.1}O_3$, $BiFe_{0.856}Cu_{0.015}Ti_{0.1}O_3$ and $BiFe_{0.85}Cu_{0.025}Ti_{0.1}O_3$.

The review of the semicircle disclosed that instead of a semicircle cantered on the real x-axis there is a depression angle. The Cole–Cole formalism is followed by the behaviour of the electrical response. Additionally, the electrical response is consists of two semicircle suggested by the shape of the curve. These circles related to electrically active regions differently. At low frequencies (<103 Hz), the grain boundary response will be obtained. The total value of the electrical response is governed by the bulk properties of the material in the high frequency range (>103 Hz). The grain boundary contribution is shown by low frequency semicircle while the grain contribution is shown by higher frequency semicircle. The other contribution in semicircle shown by depression offers more indication of distribution of relaxation times with polarization [69, 70].

The semi-circular arcs observed in plots have their centres located at the x-axis. This reveals a relaxation of non-Debye type, instead of a single relaxation process, with a dispersal of time of relaxation. The inset of figures for the respective samples clearly shows the existence of two arcs. However at higher temperature, the small arc at high frequencies is likely to be hidden by the leading larger arc at low frequencies (due to grain boundary contribution) and only a single arc is observed. The high ionic conductivity phase with the grain can be observed by small grain response and its disappearance at high temperatures may be because of the large difference between grain and grain boundary in the magnitudes of resistance. In both cases, the semi-circular arcs intercept on the x-axis is decreased with the rise of temperature. This is due to change in conductivity which is thermally activated and to increased conducting ions bounding rates. The resistance value for the grain (Rg) is equal to the intercept of the parallel semicircle with the real axis at a certain temperature [69].

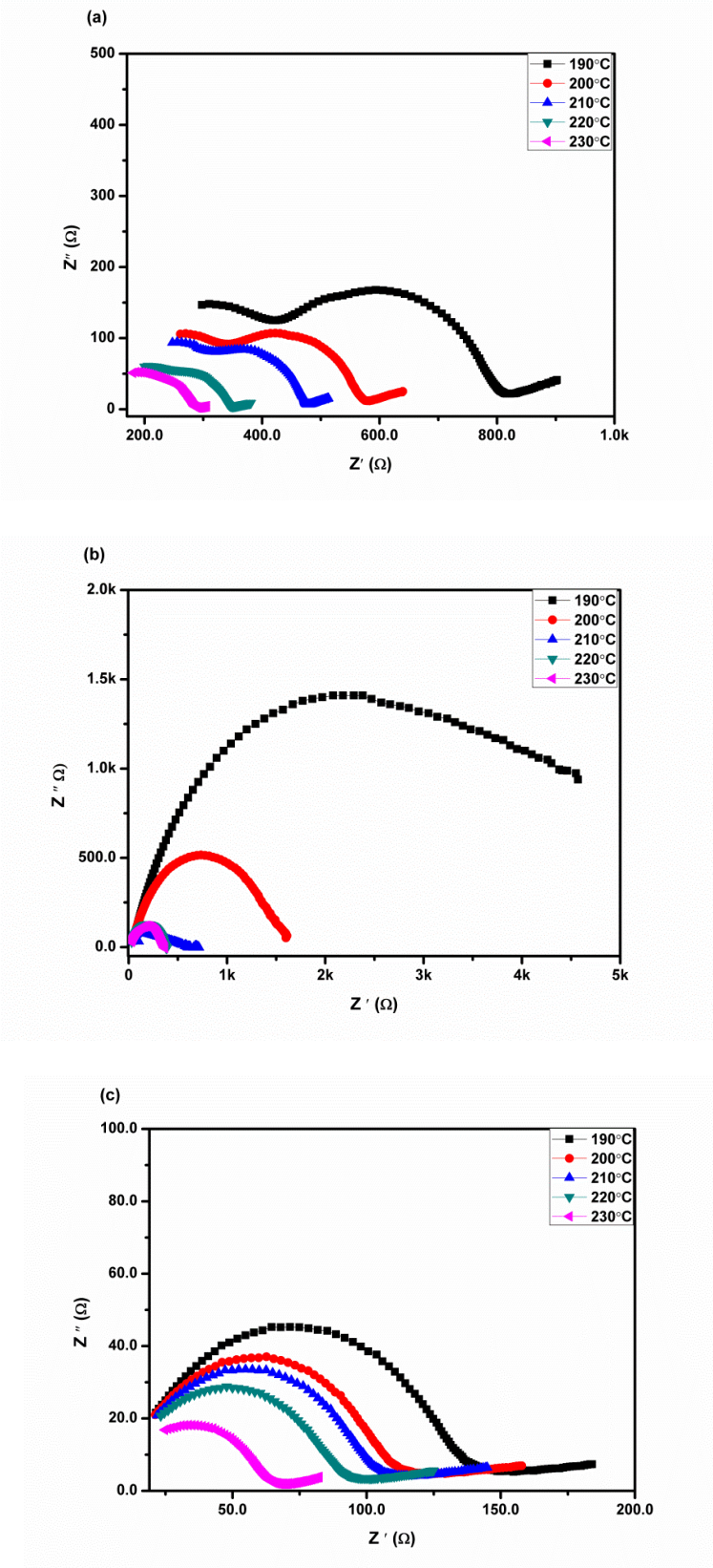

Fig. 4.4: *Nyquist Plots* $BiFe_{0.867}Cu_0Ti_{i0.1}O_3$ $BiFe_{0.856}Cu_{0.015}Ti_{0.1}O_3$ *and* $BiFe_{0.85}Cu_{0.025}Ti_{0.1}O_3$

Fig. 4.5 shows the plot of imaginary part of impedance with frequency from 100-1MHz at different temperatures. The Z′ has higher values in the low frequency region and drops monotonically as the frequency increases and rests invariant at high frequencies regardless of temperature.

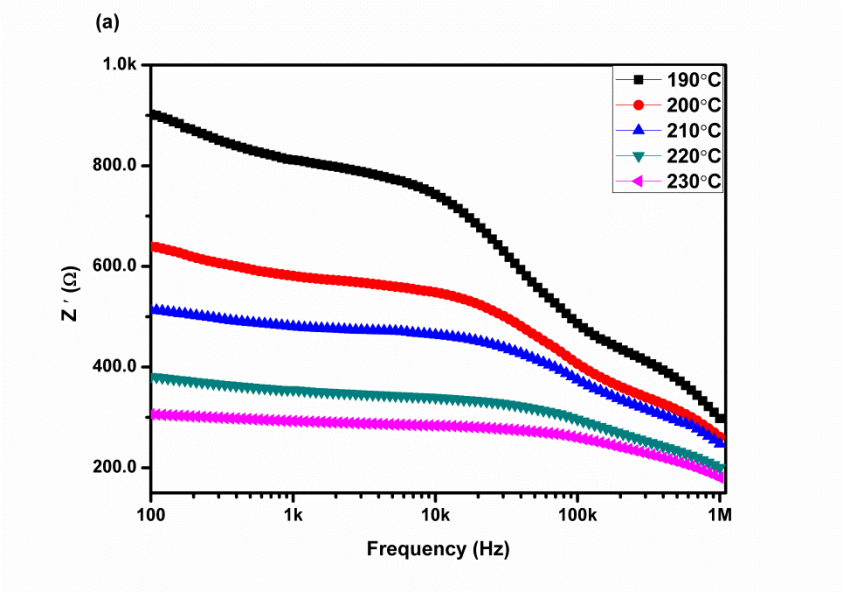

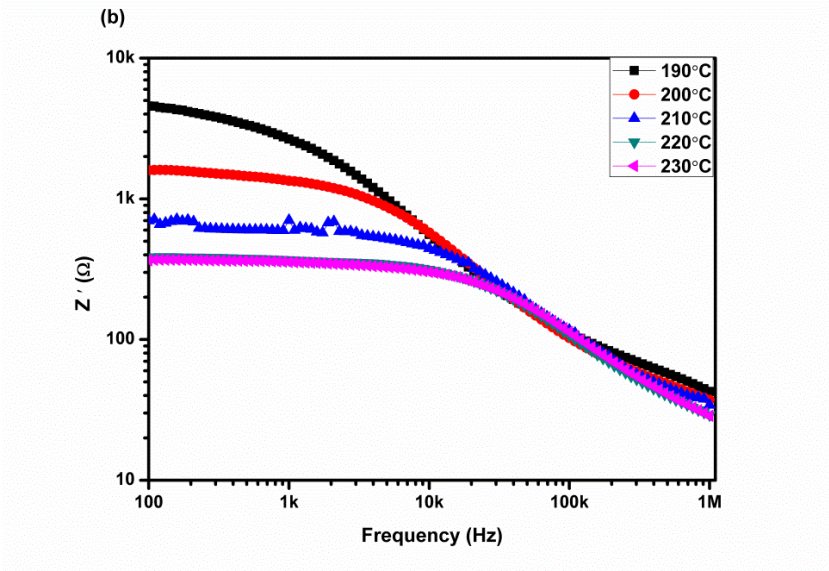

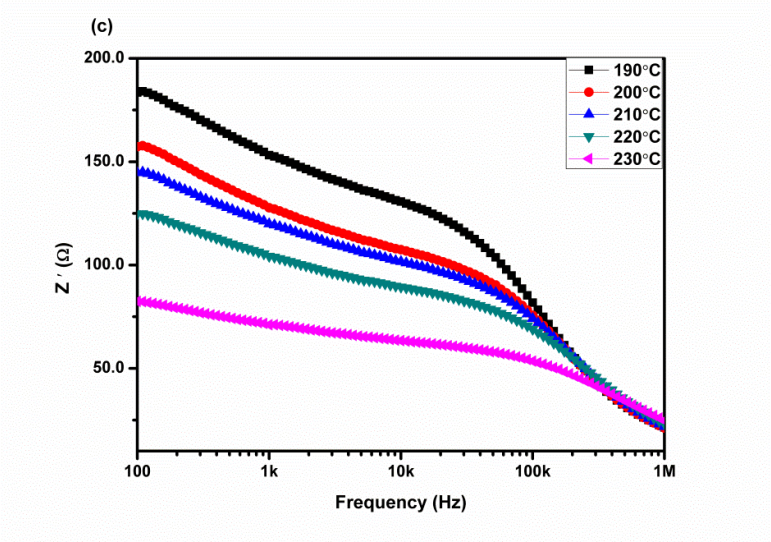

Fig. 4.5 The plot f-Z′ of a) $BiFe_{0.867}Cu_0Ti_{i0.1}O_3$,b) $BiFe_{0.856}Cu_{0.015}Ti_{0.1}O_3$ And c) $BiFe_{0.85}Cu_{0.025}Ti_{0.1}O_3$

The magnitude of resistance decreases as the temperature increases showing NTCR behaviour, which is Negative Temperature Coefficient Resistance. The values of resistance combine in higher frequency area for all temperatures. This trend may be because of ac conductivity which increases with the increasing frequency and temperature. The combining of the arcs in the high frequency region recommends a subsequent lowering of the barrier properties and conceivable discharge of space charge in the materials at all temperatures.

Fig. 4.6 shows the plot f-Z″ at different temperatures. The plot of imaginary part of impedance is appropriate for assessment of the relaxation frequency in sample.

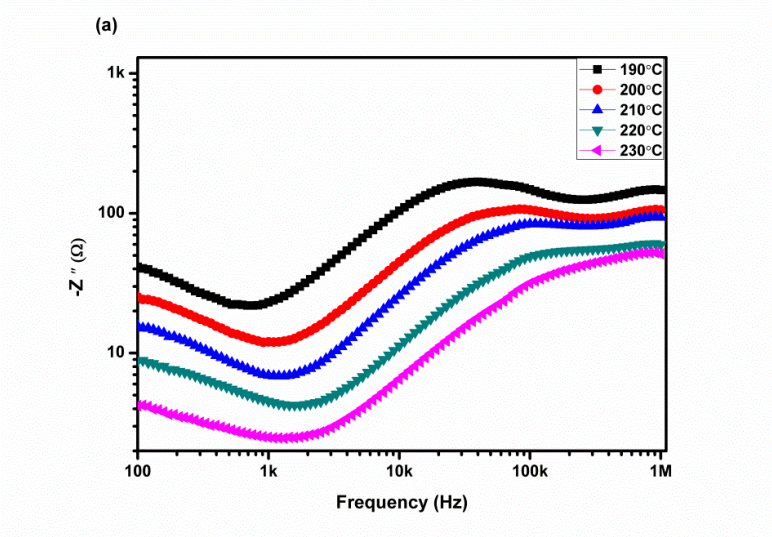

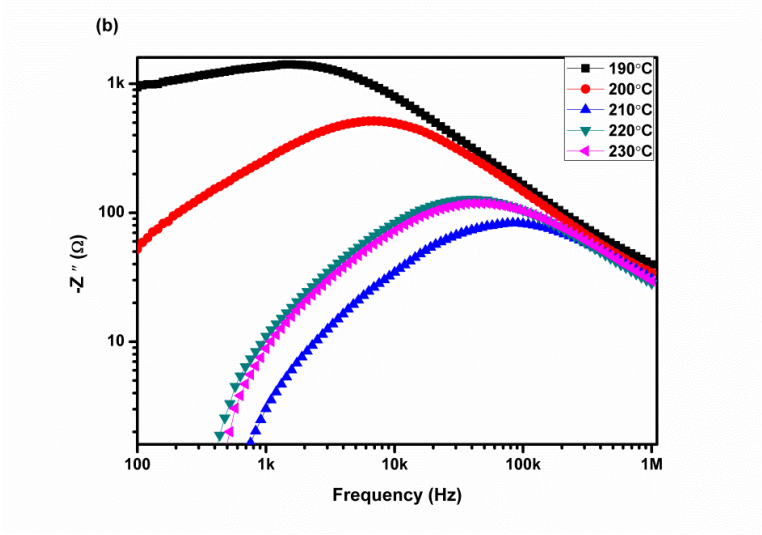

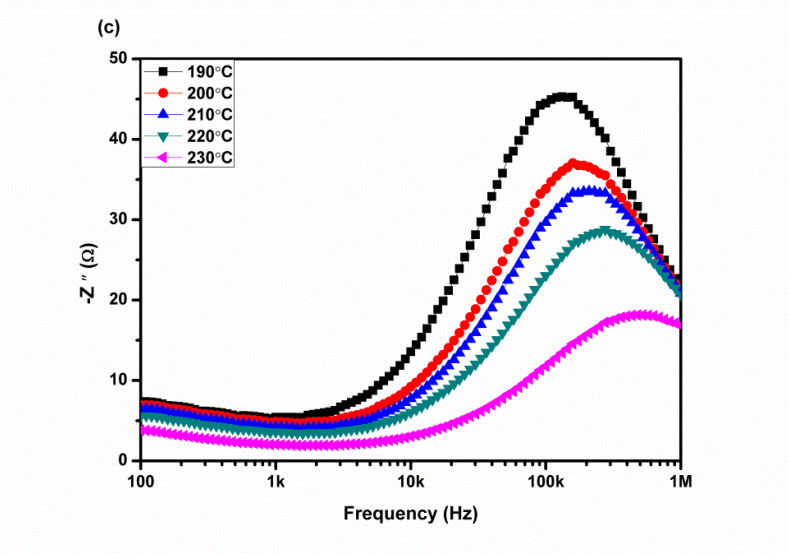

Fig. 4.6: Plot of f-Z″ for a) $BiFe_{0.867}Cu_0Ti_{0.1}O_3$,b) $BiFe_{0.856}Cu_{0.015}Ti_{0.1}O_3$ and c)$BiFe_{0.85}Cu_{0.025}Ti_{0.1}O_3$

The rising of peak and its shifting to higher frequencies is observed as the temperature increasing. The peak sifting shows the presence of relaxation in the component. The plots of Z″ versus frequency or real and imaginary part impedance are suitable for relaxation frequency determination. The presence of temperature dependent relaxation processes in the system is determined by peak broadening which is because of the increase in temperature. Because of the existence of immobile species at low temperature and imperfections at high temperature, the relaxation process occurs in the sample.

The modulus method is another method to study the electrical properties of the system. The modulus method aids the endorsement of the uncertainty rising in the system related to the grain and grain boundary effect at higher temperatures which may not be familiar from impedance graphs. The complex modulus is calculated by this relation;

$$M^* = M' + jM''$$

$M' = vC_oZ''$, $M'' = vC_oZ'$ (v = 2 pfr), C_o is geometrical capacitance = e_o A/t (e_o = free space permittivity, A = electrode surface area and t = thickness)

Fig. 4.7 the plots of M′ are shown in range of frequency from 100Hz to 1MHz at various temperatures.

M′ has very low value almost zero is perceived in the region of low frequency region. The conduction phenomena are ascribed by the continuous distribution with the increase in frequency at all the temperatures. This distribution may be because of charge carriers which have short-range of mobility.

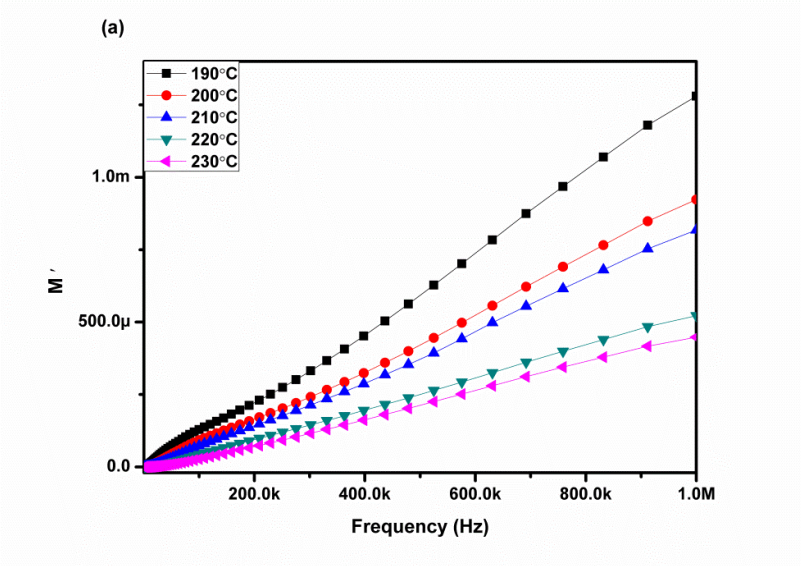

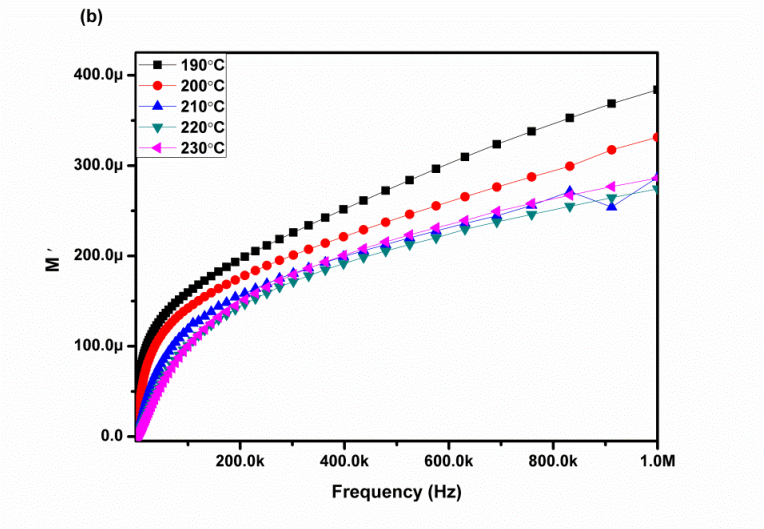

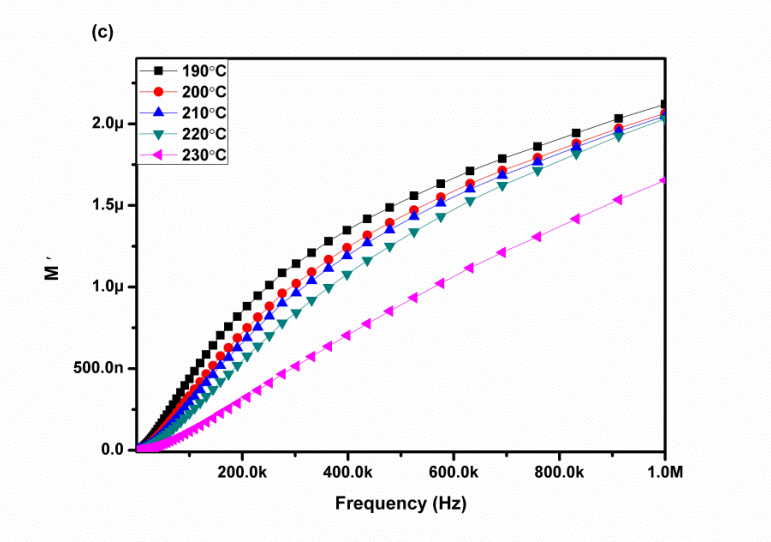

Fig 4.7: the plot of f-M' for a) $BiFe_{0.867}Cu_0Ti_{0.1}O_3$, b)$BiFe_{0.856}Cu_{0.015}Ti_{0.1}O_3$ and c)$BiFe_{0.85}Cu_{0.025}Ti_{0.1}O_3$

Fig 4.8 shows the plots of the imaginary parts of modulus. It moves towards higher relaxation frequencies as the temperature increases.

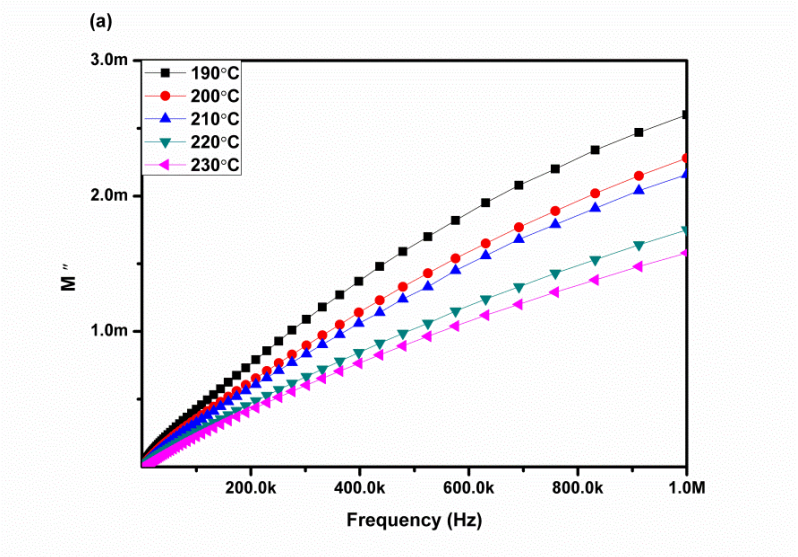

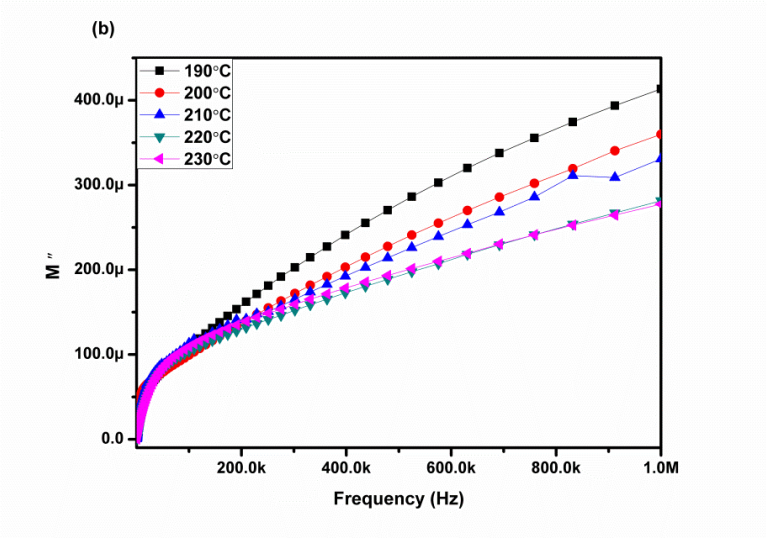

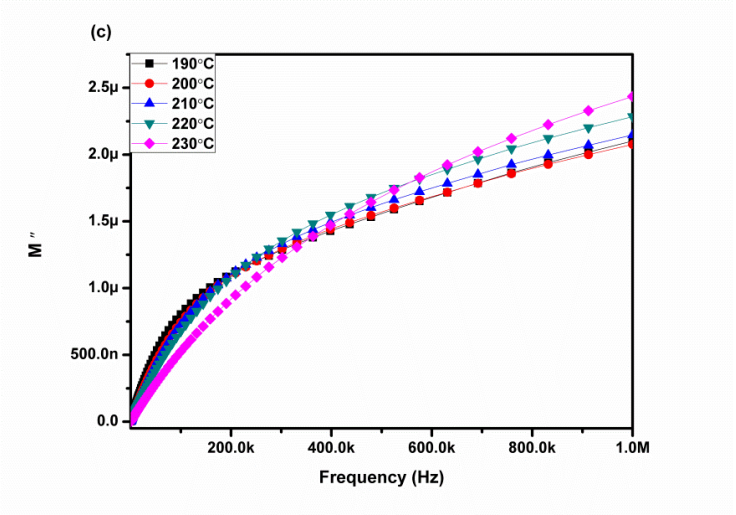

Fig. 4.8: the plot of f-M'' for a) $BiFe_{0.867}Cu_0Ti_{0.1}O_3$,b) $BiFe_{0.856}Cu_{0.015}Ti_{0.1}O_3$ and c) $BiFe_{0.85}Cu_{0.025}Ti_{0.1}O_3$

This performance shows that the charge carriers intrinsically dominate the bounding process when the dielectric relaxation is activated thermally. When the peaks expand asymmetrically, it shows the spread of relaxation with different time constant. When the temperature increases the magnitude of peaks also increases. [69]

Conclusion

Conclusion

- Cu and Ti co-doped bismuth ferrite was prepared via Solid State Mix Oxide Method.
- Room temperature XRD indexed to the BFO rhombohedral cell with the peak shift towards low diffraction angle and to the secondary phase of $Bi_2Fe_4O_9$
- Increase in density and decrease in grain size by increasing Cu contents was observed by SEM analysis.
- The different chemical bonds present in the Ti and Cu doped samples has been identified and confirmed through Fourier Transform Infrared spectroscopy.
- The complex impedance and modulus have been studied as function of frequency from 100Hz- 1MHz at temperature ranging from room temperature to 250℃ using LCR.
- The CIS data reveals that magnitude of impedance decreases with rise of temperature and frequency showing NTCR behavior.

References

1. Agrawal, S., et al., Structural, Optical, Dielectric and Magnetic Properties of Cu Doped $BiFeO_3$ Nanoparticles Synthesized by Sol Gel Method. Materials Focus, 2014. 3(1): p. 60-66.
2. Jia, D.-C., et al., Structure and multiferroic properties of $BiFeO_3$ powders. Journal of the European Ceramic Society, 2009. 29(14): p. 3099-3103.
3. Nelson, C.T., et al., Spontaneous vortex nanodomain arrays at ferroelectric heterointerfaces. Nano Letters, 2011. 11(2): p. 828-834.
4. Schmid, H., Multi-ferroic magnetoelectrics. Ferroelectrics, 1994. 162(1): p. 317-338.
5. Dong, S., et al., Microscopic model for the ferroelectric field effect in oxide heterostructures. Physical Review B, 2011. 84(15): p. 155117.
6. Khomskii, D., Trend: Classifying multiferroics: Mechanisms and effects. Physics, 2009. 2: p. 20.
7. Izyumskaya, N., Y. Alivov, and H. Morkoc, Oxides, oxides, and more oxides: High-κ oxides, ferroelectrics, ferromagnetics, and multiferroics. Critical Reviews in Solid State and Materials Sciences, 2009. 34(3-4): p. 89-179.
8. Akbashev, A.R. and A.R. Kaul, Structural and chemical aspects of the design of multiferroic materials. Russian Chemical Reviews, 2011. 80(12): p. 1159.
9. Picozzi, S. and C. Ederer, First principles studies of ic materials. Journal of Physics: Condensed Matter, 2009. 21(30): p. 303201.
10. Michel, C., et al., The atomic structure of $BiFeO_3$. Solid State Communications, 1969. 7(9): p. 701-704.
11. Kubel, F. and H. Schmid, Structure of a ferroelectric and ferroelastic monodomain crystal of the perovskite $BiFeO_3$. Acta Crystallographica Section B: Structural Science, 1990. 46(6): p. 698-702.
12. Neaton, J., et al., First-principles study of spontaneous polarization in multiferroic $BiFeO_3$. Physical Review B, 2005. 71(1): p. 014113.
13. Zhu, H., et al., Single-crystal oxide substrate dependent electrical properties of sputtered $BiFeO_3$ thin films. Materials Letters, 2016. 174: p. 57-60.
14. Wu, J. and J. Wang, Improved ferroelectric and fatigue behavior of $Bi_{0.95}Gd_{0.05}FeO_3/BiFe_{0.95}Mn_{0.05}O_3$ bilayered thin films. The Journal of Physical Chemistry C, 2010. 114(45): p. 19318-19321.
15. Zhang, J., et al., Large field-induced strains in a lead-free piezoelectric material. Nature Nanotechnology, 2011. 6(2): p. 98-102.
16. Catalan, G. and J.F. Scott, Physics and applications of bismuth ferrite. Advanced Materials, 2009. 21(24): p. 2463-2485.
17. Wang, Y., A giant polarization value in bismuth ferrite thin films. Journal of Alloys and Compounds, 2011. 509(41): p. L362-L364.
18. Wang, J., et al., Epitaxial $BiFeO_3$ multiferroic thin film heterostructures. Science, 2003. 299(5613): p. 1719-1722.
19. Yun, K.Y., M. Noda, and M. Okuyama, Prominent ferroelectricity of $BiFeO_3$ thin films prepared by pulsed-laser deposition. Applied physics letters, 2003. 83(19): p. 3981-3983.
20. Dong, G., et al., Optimization of the multiferroic $BiFeO_3$ thin films by divalent ion (Mn, Ni) co-doping at B-sites. Materials Letters, 2014. 118: p. 31-33.
21. Wang, Y., et al., Room-temperature saturated ferroelectric polarization in $BiFeO_3$ ceramics synthesized by rapid liquid phase sintering. Applied Physics Letters, 2004. 84(10): p. 1731-1733.

22. Shetty, S., V. Palkar, and R. Pinto, BiFeO3 thin films: Novel effects. PRAMANA-J. Phys, 2002. 58: p. 1027.
23. Palkar, V., J. John, and R. Pinto, Observation of saturated polarization and dielectric anomaly in magnetoelectric BiFeO 3 thin films. Applied Physics Letters, 2002. 80(9): p. 1628-1630.
24. Neirman, S.M., The Curie point temperature of $Ba(Ti_{1-x}Zr_x)O_3$ solid solutions. Journal of Materials Science, 1988. 23(11): p. 3973-3980.
25. Barsoukov, E. and J.R. Macdonald, Impedance spectroscopy: theory, experiment, and applications. 2005: John Wiley & Sons.
26. Spaldin, N.A., S.-W. Cheong, and R. Ramesh, Multiferroics: past, present, and future. Physics Today, 2010. 63(10): p. 38-43.
27. Lines, M.E. and A.M. Glass, Principles and applications of ferroelectrics and related materials. 1977: Oxford university press.
28. Smolenskiĭ, G. and I. Chupis, Ferroelectromagnets. Soviet Physics Uspekhi, 1982. 25(7): p. 475.
29. Khikhlovskyi, S.V.V. and G. Blake, The renaissance of multiferroics: bismuth ferrite ($BiFeO_3$)–a candidate multiferroic material in nanoscience. University of Groningen, 2010.
30. Damjanovic, D. and M. Demartin, Contribution of the irreversible displacement of domain walls to the piezoelectric effect in barium titanate and lead zirconate titanate ceramics. Journal of Physics: Condensed Matter, 1997. 9(23): p. 4943.
31. Damjanovic, D., Ferroelectric, dielectric and piezoelectric properties of ferroelectric thin films and ceramics. Reports on Progress in Physics, 1998. 61(9): p. 1267.
32. Busch, G. and P. Scherrer, Eine neue seignette-elektrische Substanz. Naturwissenschaften, 1935. 23(43): p. 737-737.
33. Xu, Y., et al., Ferroelectric $Sr_{0.60}Ba_{0.40}Nb_2O_6$ thin films by the sol-gel process: Electrical and optical properties. Physical Review B, 1991. 44(1): p. 35.
34. Sonin, A. and B. Strukov, Introduction to Ferroelectricity (Vysshaya Shkola, Moscow, 1970). Google Scholar: p. 272.
35. Kahn, O., Molecular Magnetism; VCH: New York, 1993. There is no corresponding record for this reference, 1996: p. 131-132.
36. Ascher, E., et al., Some Properties of Ferromagnetoelectric Nickel-Iodine Boracite, $Ni_3B_7O1_3I$. Journal of Applied Physics, 1966. 37(3): p. 1404-1405.
37. Dos Santos, A.M., et al., Evidence for the likely occurrence of magnetoferroelectricity in the simple perovskite, $BiMnO_3$. Solid State Communications, 2002. 122(1): p. 49-52.
38. Kimura, T., G. Lawes, and A. Ramirez, Electric polarization rotation in a hexaferrite with long-wavelength magnetic structures. Physical review letters, 2005. 94(13): p. 137201.
39. Kimura, T., et al., Distorted perovskite with e.g. configuration as a frustrated spin system. Physical Review B, 2003. 68(6): p. 060403.
40. Vajk, O., et al., Neutron-scattering studies of magnetism in multiferroic $HoMnO_3$. Journal of applied physics, 2006. 99(8): p. 08E301.
41. Kenzelmann, M., et al., Magnetic inversion symmetry breaking and ferroelectricity in $TbMnO_3$. Physical Review Letters, 2005. 95(8): p. 087206.
42. Goto, T., et al., Ferroelectricity and giant magnetocapacitance in perovskite rare-earth manganites. Physical review letters, 2004. 92(25): p. 257201.
43. Yokosawa, T., et al., Crystal symmetry of $BiMnO_3$: Electron diffraction study. Physical Review B, 2008. 77(2): p. 024111.

44. Shishidou, T., et al., First-principles study on the electronic structure of bismuth transition-metal oxides. Journal of Physics: Condensed Matter, 2004. 16(48): p. S5677.
45. Kiselev, S., R. Ozerov, and G. Zhdanov. Detection of magnetic order in ferroelectric $BiFeO_3$ by neutron diffraction. in Soviet Physics Doklady. 1963.
46. Teague, J.R., R. Gerson, and W.J. James, Dielectric hysteresis in single crystal $BiFeO_3$. Solid State Communications, 1970. 8(13): p. 1073-1074.
47. Belik, A.A., et al., Neutron powder diffraction study on the crystal and magnetic structures of $BiCrO_3$. Chemistry of Materials, 2008. 20(11): p. 3765-3769.
48. Kim, D.H., et al., Antiferroelectricity in multiferroic $BiCrO_3$ epitaxial films. Applied physics letters, 2006. 89(16): p. 162904.
49. Kimura, H., et al., Field-induced dielectric and magnetic phase transitions in multiferroic compounds of RMn_2O_5 (R= Er, Ho). Journal of Korean Physical Society, 2007. 51: p. 870.
50. Alonso, J., et al., High Oxygen Pressure Preparation, Structural Refinement, and Thermal Behavior of RMn_2O_5 (R== La, Pr, Nd, Sm, Eu). Journal of Solid State Chemistry, 1997. 129(1): p. 105-112.
51. Kimura, H., et al., Magnetically Induced Ferroelectricity in Multiferroic Compounds of RMn_2O_5. Ferroelectrics, 2007. 354(1): p. 77-85.
52. Hur, N., et al., Colossal Magnetodielectric Effects in $DyMn_2O_5$. Physical review letters, 2004. 93(10): p. 107207.
53. Munoz, A., et al., Magnetic structure and properties of $BiMn_2O_5$ oxide: A neutron diffraction study. Physical Review B, 2002. 65(14): p. 144423.
54. Von Wartburg, W., The magnetic structure of magnetoelectric nickel–iodine boracite $Ni_3B_7O1_3I$. physica status solidi (a), 1974. 21(2): p. 557-568.
55. Knížek, K., P. Novák, and M. Küpferling, Electronic structure and conductivity of ferroelectric hexaferrite: Ab initio calculations. Physical Review B, 2006. 73(15): p. 153103.
56. Baettig, P. and N.A. Spaldin, Ab initio prediction of a multiferroic with large polarization and magnetization. Applied Physics Letters, 2005. 86(1): p. 012505.
57. Baettig, P., C. Ederer, and N.A. Spaldin, First principles study of the multiferroics $BiFeO_3$, Bi_2FeCrO_6, and $BiCrO_3$: Structure, polarization, and magnetic ordering temperature. Physical Review B, 2005. 72(21): p. 214105.
58. Kamba, S., et al., Infrared and magnetic characterization of multiferroic Bi_2FeCrO_6 thin films over a broad temperature range. Physical Review B, 2008. 77(10): p. 104111.
59. Kadomtseva, A., et al., Phase transitions in multiferroic $BiFeO_3$ crystals, thin-layers, and ceramics: enduring potential for a single phase, room-temperature magnetoelectric 'holy grail'. Phase Transitions, 2006. 79(12): p. 1019-1042.
60. Raghavan, C., J. Kim, and S. Kim, Structural and ferroelectric properties of chemical solution deposited (Nd, Cu) co-doped $BiFeO_3$ thin film. Ceramics International, 2013. 39(4): p. 3563-3568.
61. Chakraborty, S., S. Mukherjee, and S. Mukherjee, Studies on dielectric and ferroelectric properties of pure and rare-earth doped nanocrystalline Bismuth Ferrite. Journal of The Australian Ceramic Society Volume, 2015. 51(1): p. 45-53.
62. Lawita, P., et al., Effects of Nd and Co co-doping on phase, microstructure and ferromagnetic properties of bismuth ferrite ceramics. Ceramics International, 2013. 39: p. S253-S256.

63. Takahashi, K. and M. Tonouchi, Influence of manganese doping in multiferroic bismuth ferrite thin films. Journal of Magnetism and Magnetic Materials, 2007. 310(2): p. 1174-1176.
64. Chou, C.-S., et al., Preparation and characterization of the lead-free piezoelectric ceramic of $Bi_{0.5}Na_{0.5}TiO_3$ doped with CuO. Powder technology, 2011. 210(3): p. 212-219.
65. Singh, V., et al., Structural transition, magnetic and optical properties of Pr and Ti co-doped $BiFeO_3$ ceramics. Journal of Magnetism and Magnetic Materials, 2014. 349: p. 264-267.
66. Das, R., T. Sarkar, and K. Mandal, Multiferroic properties of Ba^{2+} and Gd^{3+} co-doped bismuth ferrite: magnetic, ferroelectric and impedance spectroscopic analysis. Journal of Physics D: Applied Physics, 2012. 45(45): p. 455002.
67. Kaur, B., et al., Modifications in magnetic anisotropy of M—type strontium hexaferrite crystals by swift heavy ion irradiation. Journal of magnetism and magnetic materials, 2006. 305(2): p. 392-402.
68. Kaur, B., et al., AC Impedance Spectroscopy, Conductivity and Optical Studies of Sr doped Bismuth Ferrite Nanocomposites. International Journal of Electrochemical Science, 2016. 11(5): p. 4120-4135.
69. Coondoo, I., et al., Structural, dielectric and impedance spectroscopy studies in $(Bi_{0.90}R_{0.10})Fe_{0.95}Sc_{0.05}O_3$ [R= La, Nd] ceramics. Ceramics International, 2014. 40(7): p. 9895-9902.
70. Behera, B., P. Nayak, and R. Choudhary, Structural and impedance properties of $KBa_2V_5O_{15}$ ceramics. Materials Research Bulletin, 2008. 43(2): p. 401-410.
71. Hu, Y., et al., Synthesis of bismuth ferrite nanoparticles via a wet chemical route at low temperature. Journal of nanomaterials, 2011. 2011: p. 27.
72. Arya, G., et al., Structural, Dielectric, Ferroelectric and Magnetic Properties of Mn-doped $BifeO_3$ Nanoparticles Synthesized by Sol-gel Method. 1963.